Coexistence of superconductivity and antiferromagnetism in $(Li_{0.8}Fe_{0.2})OHFeSe$

X. F. Lu[1,2], N. Z. Wang[1,2], H. Wu[3,4], Y. P. Wu[1,2], D. Zhao[1,2], X. Z. Zeng[1,2], X. G. Luo[1,2,5], T. Wu[1,2,5], W. Bao[6], G. H. Zhang[7,8], F. Q. Huang[7,8], Q. Z. Huang[3] and X. H. Chen[1,2,5]*

Iron selenide superconductors exhibit a number of unique characteristics that are helpful for understanding the mechanism of superconductivity in high-T_c iron-based superconductors more generally. However, in the case of $A_xFe_2Se_2$ ($A = K$, Rb, Cs), the presence of an intergrown antiferromagnetic insulating phase makes the study of the underlying physics problematic. Moreover, FeSe-based systems intercalated with alkali metal ions, NH_3 molecules or organic molecules are extremely sensitive to air, which prevents the further investigation of their physical properties. It is therefore desirable to find a stable and easily accessible FeSe-based superconductor to study its physical properties in detail. Here, we report the synthesis of an air-stable material, $(Li_{0.8}Fe_{0.2})OHFeSe$, which remains superconducting at temperatures up to ∼40 K, by means of a novel hydrothermal method. The crystal structure is unambiguously determined by a combination of X-ray and neutron powder diffraction and nuclear magnetic resonance. Moreover, antiferromagnetic order is shown to coexist with superconductivity. This synthetic route opens a path for exploring superconductivity in other related systems, and confirms the appeal of iron selenides as a platform for understanding superconductivity in iron pnictides more broadly.

Tetragonal β-$Fe_{1+\delta}Se$ ($0.01 < \delta < 0.04$) exhibits superconductivity at ∼8.5 K when $\delta = 0.01$, which differs from canonical iron-based superconductors in which superconductivity arises when they closely approach the chemical stoichiometry[1,2]. Moreover, different from LnFeAsO (Ln = La, Sm; refs 3,4) or $BaFe_2As_2$ (refs 5,6), which need chemical substitution to drive the system from the antiferromagnetic state into the superconducting state, the undoped FeSe already exhibits superconductivity instead of any magnetic ordering[1,2] and the superconducting transition temperature (T_c) could be greatly improved from 8.5 K to 37 K with a hydrostatic pressure of 7 GPa (refs 7,8). Furthermore, the T_c in the one-unit-cell FeSe thin film on a $SrTiO_3$ substrate can be even higher, reaching as much as ∼65 K (refs 9–12) and greatly exceeding the bulk T_c of all known iron-based superconductors. On the other hand, the low-energy electronic structure of the heavily electron-doped $A_xFe_2Se_2$ ($A = K$, Rb, Cs) demonstrates that interband scattering or Fermi surface nesting is not a necessary ingredient for the unconventional superconductivity in iron-based superconductors[13,14], which is believed to be important in understanding the mechanism of superconductivity in FeAs-based superconductors. All the cases mentioned above suggest that FeSe-derived superconductors are good systems to investigate the mechanism of high-T_c superconductivity in the iron-based superconductors. In iron selenides, alkali metal ions and small molecules could be intercalated into two adjacent FeSe layers to enhance the superconductivity of the FeSe layers, including $A_xFe_{2-y}Se_2$ ($A = K$, Rb, Cs, and so on)[15–19], $Li_x(NH_2)_y(NH_3)_{1-y}Fe_2Se_2$ (ref. 20) and $Li_x(C_5H_5N)_yFe_{2-z}Se_2$ (ref. 21). In the case of $K_xFe_{2-y}Se_2$, the

superconducting phase without Fe vacancies is always intergrown with an insulating antiferromagnetic ordered phase, known as $K_2Fe_4Se_5$ (245 phase), with a Néel temperature as high as ∼560 K and a $\sqrt{5} \times \sqrt{5}$ order of Fe vacancies[22–24]. The intergrowth of the superconducting phase and the insulating 245 phase makes it difficult to investigate the underlying physics in this system. Moreover, for the compounds with intercalation of alkali ions and small molecules between FeSe layers[15,20], the complexity of structure introduced by the spacer layer would further hinder the investigation of the mechanism of superconductivity. Furthermore, the extreme sensitivity to air of these superconductors also prevents a number of feasible physical property measurements on these materials. Therefore, it is crucial to develop suitable FeSe-derived superconductors for physical property measurements to reveal the underlying mechanism of superconductivity among this class of intriguing compounds. Herein, we report on the comprehensive determination of the crystal structure for a novel superconductor, $(Li_{0.8}Fe_{0.2})OHFeSe$, with coexistence of superconductivity and antiferromagnetism.

The crystal structure of the sample in the present study has been determined by X-ray diffraction (XRD) of the powder compound. It adopts a structure with alternating layers of anti-PbO-type FeSe and anti-PbO-type $LiFeO_2$. All Bragg peaks of the XRD pattern can be indexed by using a tetragonal structure with space group $P4/nmm$ (No. 129), and the corresponding refinement process gives a very good R factors (for example, $R_{wp} = 0.0937$, $R_p = 0.0656$). The room-temperature lattice parameters obtained for the $LiFeO_2Fe_2Se_2$ model are 3.7926(1) Å for the a axis and 9.2845(1) Å for the c axis,

[1]Hefei National Laboratory for Physical Sciences at Microscale and Department of Physics, University of Science and Technology of China, Hefei, Anhui 230026, China. [2]Key Laboratory of Strongly-coupled Quantum Matter Physics, University of Science and Technology of China, Chinese Academy of Sciences, Hefei, Anhui 230026, China. [3]National Institute of Standards and Technology, Center for Neutron Research, 100 Bureau Dr., Gaithersburg, Maryland 20878, USA. [4]Department of Materials Science and Engineering, University of Maryland, College Park, Maryland 20742, USA. [5]Collaborative Innovation Center of Advanced Microstructures, Nanjing University, Nanjing 210093, China. [6]Department of Physics, Renmin University of China, Beijing 100872, China. [7]CAS Key Laboratory of Materials for Energy Conversion, Shanghai Institute of Ceramics, Chinese Academy of Sciences, Shanghai 200050, China. [8]Beijing National Laboratory for Molecular Sciences and State Key Laboratory of Rare Earth Materials Chemistry and Applications, College of Chemistry and Molecular Engineering, Peking University, Beijing 100871, China. *e-mail: chenxh@ustc.edu.cn

respectively. The lattice parameters a and b are very close to that (3.7734(1) Å) of β-Fe$_{1.01}$Se, whereas the c-axis is expanded by 68% compared to β-Fe$_{1.01}$Se owing to the intercalation of the LiFeO$_2$ layer as a spacer layer between two adjacent FeSe layers[25]. However, the distance between O and Se ($d_{O-Se} = 3.6028(1)$ Å) is larger than the expected value, and XRD could not provide further information. To understand the unexpectedly large space between O and Se and the corresponding detailed structure between the above two anions, subsequent neutron powder diffraction (NPD) experiments were conducted with Ge311 ($\lambda = 2.0775$ Å) and Cu311 ($\lambda = 1.5401$ Å) monochromators using the BT-1 powder diffractometer at the NIST Center for Neutron Research. Data were collected in the 2θ ranges 1.3–166.3° (Ge311) and 3–168° (Cu311) with a step size of 0.05° in the temperature range from 2.5 K to 295 K. Unfortunately, the structure model proposed based on XRD data of LiFeO$_2$Fe$_2$Se$_2$ cannot fit the observed NPD pattern well. The neutron scattering Fourier difference map on the observed patterns using the XRD proposed structure model indicated a large neutron scattering difference near the position (0.75, 0.75, 0.178), as shown in pink colour contours in Fig. 1a. The distance between the mass centre of this Fourier difference contour and the O position is about 0.95 Å, which is very close to the generally reported O–H single bond (~0.96 Å, or in the range of 0.92–0.98 Å). Also the relatively large background of the NPD pattern indicates large incoherent scattering from the possible H in the sample. Therefore, H was considered in the new structural model, with its position suggested by Fourier difference analysis, whereas H cannot be detected using the XRD method. However, analysis using NPD data indicates that no atoms are present at the $2a$ site, which should be occupied by Li/Fe on the basis of the XRD data.

The main question in discerning the difference between the structure models proposed by XRD and NPD is whether Li and H atoms exist in the same crystal structure or not. Therefore, we performed a site-selected nuclear magnetic resonance (NMR) experiment on the same samples, as NMR experiments can detect both Li and H elements, making them very suitable to solve this issue. In this case, we used ^{7}Li or ^{1}H NMR to determine which nucleus is contained in the structure. Surprisingly, both ^{7}Li and ^{1}H signals were observed and show a similar multi-peak feature at low temperature in our samples, as shown in Fig. 2. The special multi-peak structure in the NMR spectra arises from the low-temperature magnetic ordering phase, as will be confirmed by susceptibility and specific heat measurements later on. Considering the asymmetric intensity distribution around zero Knight shift, the above multi-peak structure is attributed to a ferromagnetic component along the external field direction in the (Li$_{0.8}$Fe$_{0.2}$)OH layer. As the temperature increases, both ^{7}Li and ^{1}H spectra become narrow and the multi-peak feature in the spectra disappears. On the other hand, temperature-dependent spin–spin relaxation (T_2) for both nuclei also shows a similar divergent behaviour with decreasing temperature, consistent with a magnetic phase transition. If the ^{7}Li and ^{1}H signals are from different crystal structures and not in the same crystal structure, different behaviours are expected for them. Therefore, the NMR result definitely proves that both Li and H should be contained in the same structure.

Based on the fact of having both Li and H in the same crystal structure from NMR measurements and random occupation of Li/Fe at $2a$ sites, we can understand the distinct structure models proposed by XRD and NPD. The scattering factor of the lightest H element is too small to be detected by XRD. In addition, the total neutron scattering from the $2a$ site could be zero when the refined fraction of Li and Fe on that site is 0.81(1) and 0.19(1), respectively (the neutron scattering amplitudes are −2.03 fm for Li and 9.54 fm for Fe). The Li/Fe ratio of 0.81(1)/0.19(1) at the $2a$ site is also confirmed by the chemical composition using inductively coupled plasma mass spectrometry. Using the new structure model
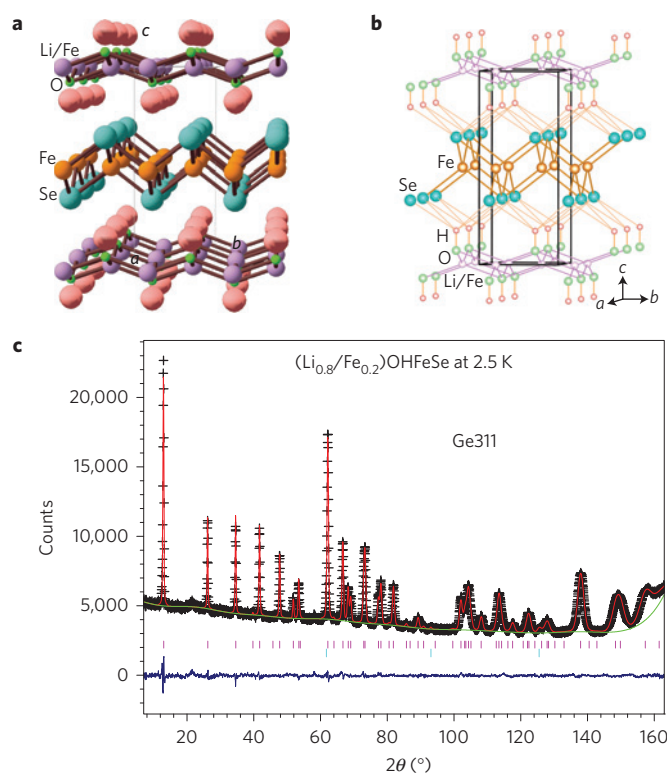
Figure 1 | Crystal structure and Rietveld refinement against NPD data for (Li$_{0.8}$Fe$_{0.2}$)OHFeSe. a, Neutron scattering Fourier difference analysis using the 2.5 K NPD data. Fourier difference contours are highlighted in pink. Oxygen atoms (green), Li/Fe atoms (purple). **b**, A schematic view of the structure of (Li$_{0.8}$Fe$_{0.2}$)OHFeSe. In the model the anti-PbO-type FeSe layers and the (Li$_{0.8}$Fe$_{0.2}$)OH layers stack alternately. **c**, Observed (crosses) and calculated (red solid line) NPD pattern for (Li$_{0.8}$Fe$_{0.2}$)OHFeSe ($\lambda = 2.0775$ Å) at 2.5 K. Differences between the observed and calculated intensities are shown at bottom of the figure. Bragg peak positions are indicated by short purple vertical bars below the NPD patterns.

containing both of Li and H, namely (Li$_{0.8}$Fe$_{0.2}$)(OH)(FeSe) (Fig. 1b), the NPD patterns in the temperature range from 2.5 K to 295 K can be perfectly fitted with excellent goodness of fit factors (Supplementary Table 1). A plot of the observed and calculated intensities measured at 2.5 K using the Ge311 monochromator ($\lambda = 2.0775$ Å) is shown in Fig. 1c and the refined structure parameters are listed in Table 1.

In the new structure model, at 295 K the O–H bond distance is 0.94 Å, while the H–Se distance is 3.078 Å. Compared with a H–Se distance of 2.75 Å observed in Li$_{0.6}$(ND$_2$)$_{0.2}$(ND$_3$)$_{0.8}$Fe$_2$Se$_2$ (ref. 20), the much larger H–Se distance in (Li$_{0.8}$Fe$_{0.2}$)OHFeSe suggests a much weaker hydrogen bonding interaction between (Li$_{0.8}$Fe$_{0.2}$)(OH) layers and FeSe layers. Moreover, the Se–Fe–Se bond angles are 103.2(2)°(×2) in (Li$_{0.8}$Fe$_{0.2}$)OHFeSe, which is smaller than 103.9°(×2) in β-Fe$_{1+\delta}$Se. Furthermore, the Fe–Se bond distance of 2.416 Å in (Li$_{0.8}$Fe$_{0.2}$)OHFeSe is larger than the 2.3958 Å in β-Fe$_{1+\delta}$Se. All these structural changes indicate that (Li$_{0.8}$Fe$_{0.2}$)OHFeSe possesses a very distorted FeSe$_4$ tetrahedron, which is compressed in the ab plane. Such a distorted FeSe$_4$ tetrahedron has also been observed in Li$_{0.6}$(NH$_2$)$_{0.2}$(NH$_3$)$_{0.8}$Fe$_2$Se$_2$, with a T_c of 43 K. It implies that distortion of the tetrahedron in FeSe-derived superconductors may enhance the superconductivity; in contrast to that in FeAs-based superconductors, in which the ideal FeAs$_4$ tetrahedron is favourable for superconductivity. Finally, different from Fe$_{1+\delta}$Se, there is no crystal structure transition observed between 295 K and 2.5 K in (Li$_{0.8}$Fe$_{0.2}$)OHFeSe.

a, ^{7}Li spectra @10.0 T
$f_0 = 165.471$ MHz
5.5 K
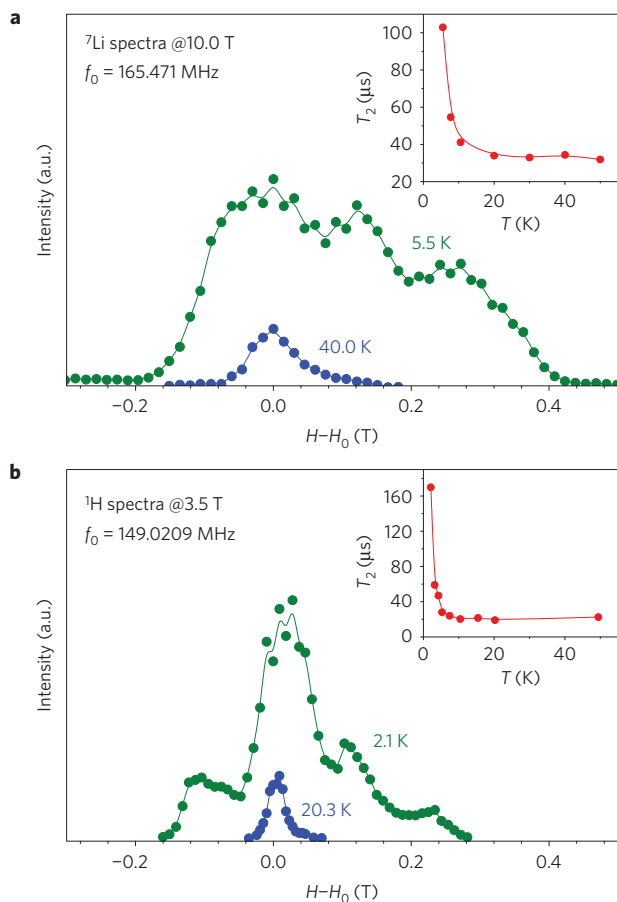40.0 K

b, ^{1}H spectra @3.5 T
$f_0 = 149.0209$ MHz
2.1 K
20.3 K

Figure 2 | Evidence for Li and H in the same structure from the NMR experiment. a, Temperature-dependent ^{7}Li NMR spectra under an external magnetic field $H = 10.0$ T. The inset shows the temperature-dependent T_2 with a NMR frequency $f_0 = 165.471$ MHz. **b**, Temperature-dependent ^{1}H NMR spectra under an external magnetic field $H = 10.0$ T. The inset shows the temperature-dependent T_2 with a NMR frequency $f_0 = 149.0209$ MHz.

Table 1 | Crystallographic parameters from the NPD refinement of $(Li_{0.8}Fe_{0.2})OHFeSe$ at 2.5 K.

Atom	Wyckoff site	x	y	z	Occupation	Uiso ($\times 100$ Å^2)
H	2c	0.75	0.75	0.1734(3)	1.00	2.79(8)
O	2c	0.25	0.25	−0.0764(1)	1.00	0.27(4)
Li/Fe$_1$	2a	0.75	0.25	0	0.81/0.19(1)	0.8
Fe$_2$	2b	0.75	0.25	0.5	1.00	0.52(2)
Se	2c	0.25	0.25	0.3390(1)	1.00	0.35(3)

Interatomic distances (Å)

Fe$_2$–Se 2.4026(8) $\times$ 4
Fe$_1$/Li–O 2.0149(6) $\times$ 4
H–Se 3.068(2) $\times$ 4
O–H 0.889(5)

Interatomic angles (°)

Se^{top}–Fe$_2$–Se^{top} 103.70(5) $\times$ 2
Se^{top}–Fe$_2$–Se^{bottom} 112.43(3) $\times$ 4
O^{top}–Li/Fe$_1$–O^{top} 139.3(1) $\times$ 2
O^{top}–Li/Fe$_1$–O^{bottom} 96.94(3) $\times$ 4
O–H–Se 119.43(6) $\times$ 4

Space group: $P4/nmm$ (No. 129); $a = b = 3.77871(4)$ Å, $c = 9.1604(1)$ Å, $V = 130.7981$ Å^3, $R_{wp} = 0.0183$, $R_p = 0.015$, $\chi^2 = 1.498$. Uiso is the isotropic displacement parameter. Owing to the total neutron scattering amplitude for the 2a site being close to zero, the temperature factor for this site was fixed at 0.8.

Figure 3a shows the temperature dependence of the magnetic susceptibility χ with an external magnetic field of 10 Oe. The as-synthesized sample shows a diamagnetic transition at approximately 40 K with a considerable shielding fraction of 60% at 2 K in the zero-field-cooling process, indicating bulk superconductivity. To identify the carrier type in $(Li_{0.8}Fe_{0.2})OHFeSe$, the temperature-dependent Seebeck coefficient was measured, as shown in Fig. 3b. The Seebeck coefficient retains a negative value in the whole temperature range from 4.5 to 300 K, indicating that electron-type carriers dominate in $(Li_{0.8}Fe_{0.2})OHFeSe$. The absolute value of thermoelectric power ($|S|$) is 6.27 μV K^{-1} at 300 K. It increases with decreasing temperature and reaches a maximum of 60 μV K^{-1} at ~140 K. Such a dome-like behaviour has been observed in other iron-based superconductors, including LnFe$_{1-x}$Co$_x$AsO (Ln = La and Sm)[26], β-FeSe (ref. 27) and K$_x$Fe$_{2-y}$Se$_2$ (ref. 28). A rapid decrease in the absolute value of thermoelectric power takes place at 40 K, with the thermoelectric power finally reaching zero below T_C in the superconducting state, consistent with the corresponding measurement of magnetic susceptibility.

The magnetic susceptibility (χ) as a function of temperature from 2 K to 300 K under an external field of 1 T for the as-synthesized samples is shown in Fig. 4a. The superconducting signal seems to be completely suppressed under this field. The temperature-dependent magnetic susceptibility exhibits a Curie–Weiss behaviour above 10 K, while a sudden decrease occurs

in the zero-field cooling (ZFC) curve around 8.5 K. The field-cooling (FC) and ZFC magnetic susceptibilities also bifurcate at roughly the same temperature. It suggests a weak ferromagnetic component due to a canted antiferromagnetic order, as derived from NMR measurements. To confirm the magnetic transition, thermodynamic measurements were performed. Figure 4b shows the temperature-dependent specific heat under different magnetic fields. Specific heat begins to rise at approximately 8.5 K and shows a peak-like feature due to magnetic ordering, which is consistent with the transition temperature from the magnetic susceptibility. Such a peak-like feature is suppressed with increasing magnetic fields and becomes very obscure as the field increases up to 9 T. Suppression of the specific heat jump by a magnetic field suggests that the magnetic order should be antiferromagnetic. The NMR experiment also indicates that the canted antiferromagnetic order originates from the $(Li_{0.8}Fe_{0.2})OH$ layer and the antiferromagnetic could coexist with superconductivity. However, this antiferromagnetic order could not be observed in the NPD experiment because of the small magnetic moment. A high-quality single crystal is thus needed to reveal the magnetic ordering structure by neutron scattering measurements. It is the ferromagnetic component induced by the external magnetic field that creates an internal field to completely suppress the Meissner effect under 1 T, such that no diamagnetic signal is observed in the susceptibility, as shown in Fig. 4a.

We successfully synthesized a new FeSe-derived superconductor, $(Li_{0.8}Fe_{0.2})OHFeSe$, with a T_c of ~40 K by a novel hydrothermal synthesis method. Using a combination of powder XRD and NPD and NMR, the structure of $(Li_{0.8}Fe_{0.2})OHFeSe$ was unambiguously determined. With alternate stacking of $(Li_{0.8}Fe_{0.2})OH$ layers and anti-PbO type FeSe layers, there exists a weak hydrogen bonding interaction between the layers. In comparison with β-Fe$_{1+\delta}$Se, the FeSe$_4$ tetrahedron is extremely compressed in the ab plane in $(Li_{0.8}Fe_{0.2})OHFeSe$. Such a distorted FeSe$_4$ tetrahedron is likely to play a key structural role in enhancing the superconductivity in FeSe-based superconductors. Furthermore, Seebeck coefficient measurements reveal that electron-type carriers dominate in this
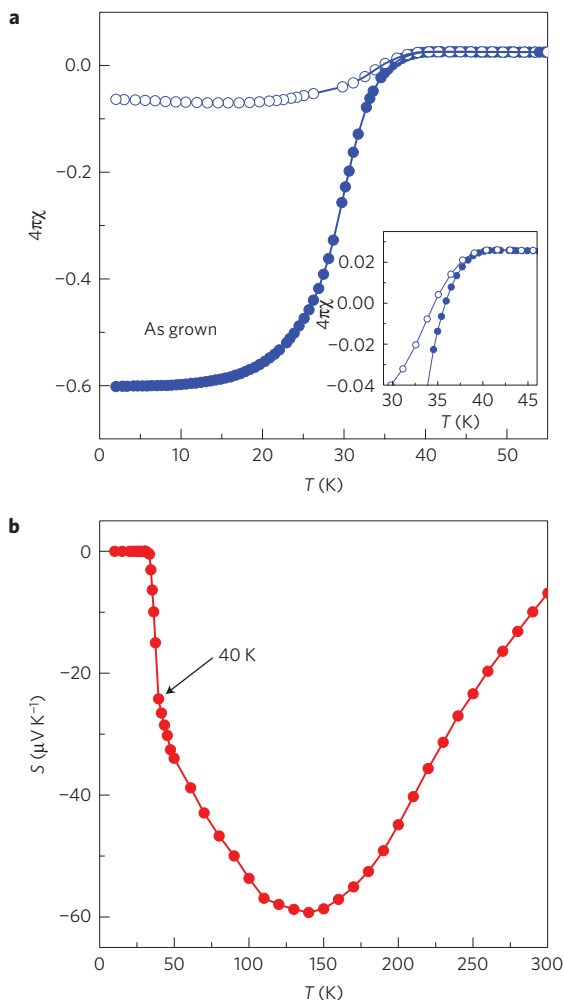
Figure 3 | Superconducting properties of $(Li_{0.8}Fe_{0.2})OHFeSe$.
a, Temperature dependence of the magnetic susceptibility χ for the as-synthesized $(Li_{0.8}Fe_{0.2})OHFeSe$ sample. Data were collected under a magnetic field of 10 Oe. The inset is a zoom-in view around the superconducting transition of the as-synthesized sample.
b, Temperature-dependent thermoelectric power of the as-synthesized $(Li_{0.8}Fe_{0.2})OHFeSe$ sample.

Figure 4 | Evidence for antiferromagnetic transition in $(Li_{0.8}Fe_{0.2})OHFeSe$.
a, Magnetic susceptibility (χ) as a function of temperature for the as-synthesized $(Li_{0.8}Fe_{0.2})OHFeSe$ sample from 2 to 300 K with an external field of 1 T. **b**, Specific heat of $(Li_{0.8}Fe_{0.2})OHFeSe$ under different external fields.

material, in accordance with the refined composition, which indicates a charge transfer from the $(Li_{0.8}Fe_{0.2})OH$ layer to the FeSe layer. Susceptibility, specific heat and NMR measurements indicate that a canted antiferromagnetic order occurs at ~ 8.5 K, and coexists with superconductivity at ~ 40 K. Different from other FeSe-derived superconductors, which are extremely sensitive to air, the $(Li_{0.8}Fe_{0.2})OHFeSe$ superconductor is air stable. The high-quality single crystal is expected to be very useful in studying the underlying physics of high-T_c iron-based superconductors.

Methods

Sample synthesis. Polycrystalline $(Li_{0.8}Fe_{0.2})OHFeSe$ samples were prepared by the hydrothermal reaction method. 0.012–0.02 mol selenourea (Alfa Aesar, 99.97% purity), 0.0075 mol Fe powder (Aladdin Industrial, analytical reagent purity), and 12 g $LiOH \cdot H_2O$ (Sinopharm Chemical Reagent, analytical reagent purity) were put into a Teflon-lined steel autoclave (50 ml) and mixed together with 10 ml de-ionized water. The Teflon-lined autoclave was then tightly sealed and heated at 160 °C for three to ten days. Shiny, lamellar polycrystalline samples were acquired from the reaction system, which were then washed repeatedly with de-ionized water and dried at room temperature.

Structure characterization and composition determination. XRD data were collected at room temperature using an X-ray diffractometer (SmartLab-9,
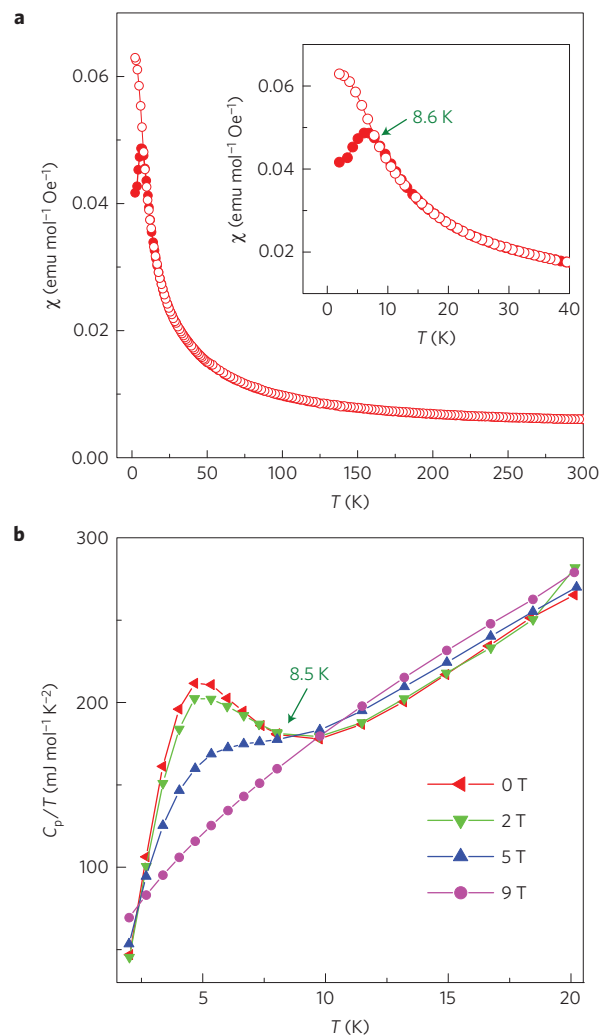
Rikagu) with Cu Kα radiation and a fixed graphite monochromator with the 2θ range 5–80° and a scanning rate of 0.1° min^{-1}. NPD experiments were conducted using Ge311 ($\lambda = 2.0775$ Å) and Cu311 ($\lambda = 1.5401$ Å) monochromators, respectively. Data were collected over the 2θ ranges 1.3–166.3°(Ge311) and 3–168°(Cu311) with a step size of 0.05° from 2.5 K to 295 K. The NPD experiments were carried out in the NIST Center for Neutron Research. The content of Li and Fe was determined by inductively coupled plasma mass spectrometry. The result indicates that the atomic ratio of Li:Fe is 0.78:1.19 with an instrument error of 0.2%. Energy dispersive X-ray analysis measurements determined the atomic ratio of Fe:Se to be 1.23(4):1 with an uncertainty $\sim$3% (Supplementary Fig. 5). Furthermore, the absolute H content in the sample was determined to be $0.7(1) \pm 0.1$ wt% by means of a CHN element analyser, which is consistent with the H content of 0.60 wt% from the chemical formula $(Li_{0.8}Fe_{0.2})OHFeSe$. The results on composition obtained from all chemical analysis mentioned above are self-consistent, and in good accordance with the composition acquired from structural refinement. These results indicate that the composition of the novel superconductor is $(Li_{0.8}Fe_{0.2})OHFeSe$. The composition indicates no Li/H site sharing.

Purity of the phase and the reproducibility of the synthesis method. No impurity could be detected by XRD, NPD or chemical analysis. There are no extra peaks observed in the XRD and NPD patterns other than those of $(Li_{0.8}Fe_{0.2})OHFeSe$. The synthesis method is highly reproducible (nearly 100%), with all samples obtained from every synthesis showing nearly the same T_C with a shielding fraction of 60% or higher.

References

1. Hsu, F. C. *et al.* Superconductivity in the PbO-type structure α-FeSe. *Proc. Natl Acad. Sci. USA* **105,** 14262–14264 (2008).
2. McQueen, T. M. *et al.* Extreme sensitivity of superconductivity to stoichiometry in $Fe_{1+\delta}Se$. *Phys. Rev. B* **79,** 014522 (2009).
3. Kamihara, Y., Watanabe, T., Hirano, M. & Hosono, H. Iron-based layered superconductor $La[O_{1-x}F_x]FeAs(x = 0.05 - 0.12)$ with $T_C = 26$ K. *J. Am. Chem. Soc.* **130,** 3296–3297 (2008).
4. Chen, X. H. *et al.* Superconductivity at 43 K in $SmFeAsO_{1-x}F_x$. *Nature* **453,** 761–762 (2008).
5. Rotter, M., Tegel, M. & Johrendt, D. Superconductivity at 38 K in the iron arsenide $Ba_{1-x}K_xFe_2As_2$. *Phys. Rev. Lett.* **101,** 107006 (2008).
6. Sasmal, K. *et al.* Superconducting Fe-based compounds $(A_{1-x}Sr_x)Fe_2As_2$ with A = K and Cs with transition temperature up to 37 K. *Phys. Rev. Lett.* **101,** 107007 (2008).
7. Margadonna, S. *et al.* Pressure evolution of the low-temperature crystal structure and bonding of the superconductor FeSe ($T_C = 37$ K). *Phys. Rev. B* **80,** 064506 (2009).
8. Medvedev, S. *et al.* Electronic and magnetic phase diagram of β-$Fe_{1.01}Se$ with superconductivity at 36.7 K under pressure. *Nature Mater.* **8,** 630–633 (2009).
9. Wang, Q. Y. *et al.* Interface-induced high-temperature superconductivity in single unit-cell FeSe films on $SrTiO_3$. *Chin. Phys. Lett.* **29,** 037402 (2012).
10. Liu, D. F. *et al.* Electronic origin of high-temperature superconductivity in single-layer FeSe superconductor. *Nature Commun.* **3,** 931 (2012).
11. He, S. L. *et al.* Phase diagram and electronic indication of high-temperature superconductivity at 65 K in single-layer FeSe films. *Nature Mater.* **12,** 605–610 (2013).
12. Tan, S. Y. *et al.* Interface-induced superconductivity and strain-dependent spin density waves in $FeSe/SrTiO_3$ thin films. *Nature Mater.* **12,** 634–640 (2013).
13. Zhang, Y. *et al.* Nodeless superconducting gap in $A_xFe_2Se_2$ (A = K, Cs) revealed by angle-resolved photoemission spectroscopy. *Nature Mater.* **10,** 273–277 (2011).
14. Qian, T. *et al.* Absence of a holelike Fermi surface for the iron-based $K_{0.8}Fe_{1.7}Se_2$ superconductor revealed by angle-resolved photoemission spectroscopy. *Phys. Rev. Lett.* **106,** 187001 (2011).
15. Guo, J. G. *et al.* Superconductivity in the iron selenide $K_xFe_2Se_2(0 \le x \le 1.0)$. *Phys. Rev. B* **82,** 180520(R) (2010).
16. Wang, A. F. *et al.* Superconductivity at 32 K in single-crystalline $Rb_xFe_{2-y}Se_2$. *Phys. Rev. B* **83,** 060512(R) (2011).
17. Krzton-Maziopa, A. *et al.* Synthesis and crystal growth of $Cs_{0.8}(FeSe_{0.98})_2$: A new iron-based superconductor with $T_C = 27$ K. *J. Phys. Condens. Matter* **23,** 052203 (2011).
18. Ying, T. P. *et al.* Observation of superconductivity at 30 K $\sim$ 46 K in $A_xFe_2Se_2$ (A = Li, Na, Ba, Sr, Ca, Yb, and Eu). *Sci. Rep.* **2,** 426 (2012).
19. Sun, L. L. *et al.* Re-emerging superconductivity at 48 kelvin in iron chalcogenides. *Nature* **483,** 67–69 (2012).
20. Burrard-Lucas, M. *et al.* Enhancement of the superconducting transition temperature of FeSe by intercalation of a molecular spacer layer. *Nature Mater.* **12,** 15–19 (2013).
21. Krzton-Maziopa, A. *et al.* Synthesis of a new alkali metal–organic solvent intercalated iron selenide superconductor with $T_c \approx 45$ K. *J. Phys. Condens. Matter* **24,** 382202 (2012).
22. Li, W. *et al.* Phase separation and magnetic order in K-doped iron selenide superconductor. *Nature Phys.* **8,** 126–130 (2012).
23. Bao, W. *et al.* A novel large moment antiferromagnetic order in $K_{0.8}Fe_{1.6}Se_2$ superconductor. *Chin. Phys. Lett.* **28,** 086104 (2011).
24. Wang, Z. W. *et al.* Structural phase separation in $K_{0.8}Fe_{1.6+x}Se_2$ superconductors. *J. Phys. Chem. C* **116,** 17847 (2012).
25. Lu, X. F. *et al.* Superconductivity in $LiFeO_2Fe_2Se_2$ with anti-PbO-type spacer layers. *Phys. Rev. B* **89,** 020507(R) (2013).
26. Wang, C. *et al.* Effects of cobalt doping and phase diagrams of $LFe_{1-x}Co_xAsO$ (L = La and Sm). *Phys. Rev. B* **79,** 054521 (2009).
27. Song, Y. J. *et al.* The pseudogap behavior in the stoichiometric FeSe superconductor ($T_c \sim 9.4$ K). *J. Korean Phys. Soc.* **59,** 312 (2011).
28. Yan, Y. J. *et al.* Electronic and magnetic phase diagram in $K_xFe_{2-y}Se_2$ superconductors. *Sci. Rep.* **2,** 212 (2011).

Acknowledgements

Author contributions

X.F.L. and N.Z.W. contributed equally to this work. X.F.L. and N.Z.W. performed sample synthesis, composition determination, susceptibility, specific heat, X-ray diffraction and thermoelectric power measurements with assistance from X.Z.Z. and X.G.L., Q.Z.H., H.W. and W.B. performed NPD experiments and carried out the structure analysis. Y.P.W., D.Z. and T.W. performed NMR experiments and analysed data. G.H.Z. and F.Q.H. carried out the refinement on XRD. X.F.L., N.Z.W., Q.Z.H., T.W. and X.H.C. analysed the data and wrote the paper. X.H.C. conceived and coordinated the project, and is responsible for the infrastructure and project direction. All authors discussed the results and commented on the manuscript.

Additional information

Supplementary information is available in the online version of the paper. Reprints and permissions information is available online at www.nature.com/reprints. Correspondence and requests for materials should be addressed to X.H.C.

Competing financial interests

The authors declare no competing financial interests.